

CHAPTER 6

Two-dimensional Hybrid Inorganic-Organic Perovskites: Methylammonium Lead Iodide

6.1 Introduction

Perovskites are the most extensively studied materials due to their unique properties such as superconductivity, pyro and piezo electricity, linear and non-linear di-electricity, insulator-metal transition, ionic conduction characteristics and ferroelectricity.¹⁻⁵ The natural occurring mineral calcium titanate (CaTiO_3) discovered by Gustav Rose in 1839 is the first member of perovskite family and acquired name from Russian mineralogist Lev Aleksevich Von Perovski.⁶ The ground state of CaTiO_3 possesses orthorhombic structure that further transforms to cubic symmetry at higher temperature with structural stoichiometry ABO_3 .⁷⁻⁹ The generalized stoichiometric formula of perovskite materials is ABX_3 , where A is a cation with larger atomic radius that forms closely packed layers with oxygen or halide anions and B is a cation with smaller atomic radius forms an arrangement of an octahedrally coordinated hole between the close-packed layers. The ideal crystal structure of perovskite materials is a cubic structure. The stable low symmetry structure of perovskite materials is due to octahedral tilting.¹⁰⁻¹² However, for stability with respect to anions and cations, the concept of tolerance factor was first introduced by Megwan and further modified by Goldschmidt and accepted universally.^{13,14} The lower value of tolerance factor “t” leads to lower symmetry. For cubic structure tolerance factor is one. Series of ideal perovskites have been discovered in past few years, such as SrTiO_3 , BaTiO_3 , CaTiO_3 , CsSnBr_3 etc.¹⁵⁻¹⁸ Amongst all these materials the CsSnX_3 and CsSnPbX_3 ($X = \text{Cl, Br, I}$) have gained a lot of interest in the recent time due to their strong photoluminescence and for solar cell applications. In 1978, Weber showed that the CsSnBr_3 has cubic structure while CsPbI_3 has low dimensional structure at normal condition due to the smaller size of Cs atom.

CHAPTER 6

Two-dimensional Hybrid Inorganic-Organic Perovskites: Methylammonium Lead Iodide

However, this is not enough to fill the space of Pb(II) perovskite structure and leads to octahedral symmetry as per the crystal field energy preference.¹⁹ To overcome this drawback and to have ideal perovskite structure, Weber successfully synthesized more stable version of perovskite material by replacing the Cs ion with Methylammonium (MA) ion in the inorganic base frame of Pb cage (see Fig. 6.1).

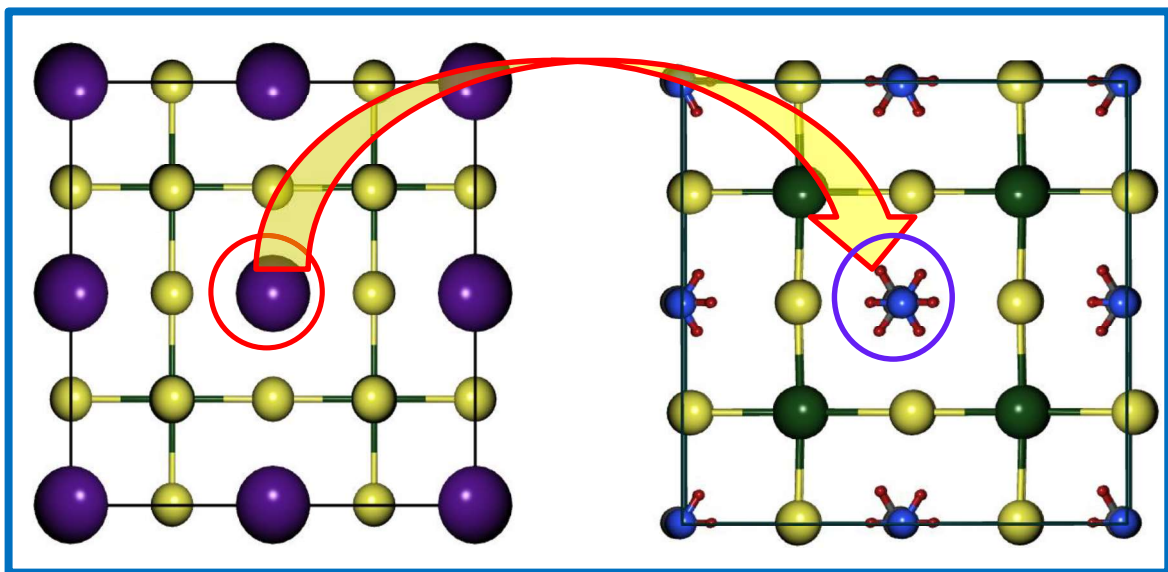


Figure 6.1: Crystal structure of (a) CsPbI₃ and (b) CH₃NH₃PbI₃.

The new class of perovskite families emerging from these changes are known as organic-inorganic hybrid perovskites. The methylammonium lead iodide (MAPI) has gained significant amount of attention of researchers due to its high solar efficiency of about 3.8 % after its first discovery.²⁰ However, within past ten years, its efficiency has risen up to 23.0 %.²¹ Therefore, the new hybrid inorganic-organic perovskite poses a new hope for maximum efficiency of solar cell. Fig. 6.1 presents the stability of different phases of perovskite with their corresponding temperature and tolerance factor. One of the major reasons for this efficiency increase can be

CHAPTER 6

Two-dimensional Hybrid Inorganic-Organic Perovskites: Methylammonium Lead Iodide

the enhancement of tolerance factor t . The organic molecule Methylammonium plays a vital role to increase the tolerance factor in parent CsPbI_3 perovskite structure.²² Many studies are carried out to understand the role of Methylammonium ions in terms of stability and electronic properties of Methylammonium lead iodide (MAPI). Incorporation of methylammonium ions

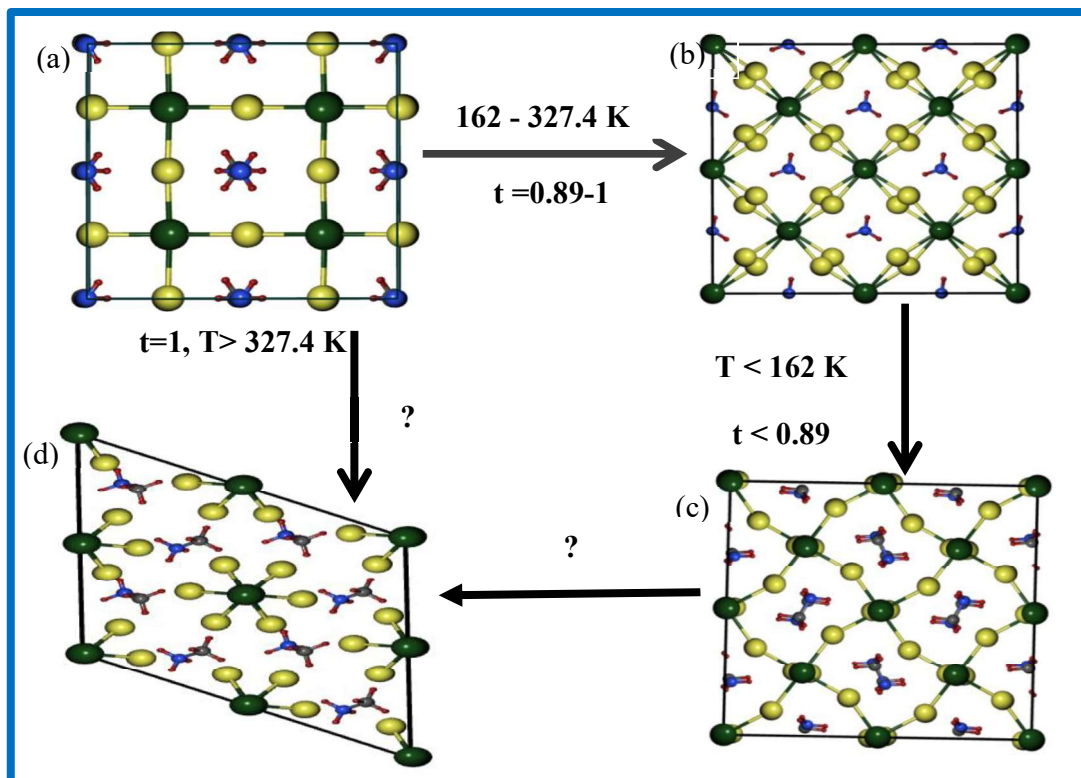


Figure 6.2: crystal structure of MAPI (a) cubic, (b) tetragonal, (c) orthorhombic and (d) hexagonal.

distorts the conventional cubic structure of the perovskite due to its rotation and resulting into lower dimensional symmetry structure.^{11,23} In addition, MAPI exhibits low symmetry structure due to the tilting or distortion of BX_6 octahedral which leads to stable configuration. These can be attributed to the slight rotation and displacement of constituent atoms or molecules at definite temperature that can determine octahedral factor.²⁴ This is the reason why cubic structure at

CHAPTER 6

Two-dimensional Hybrid Inorganic-Organic Perovskites: Methylammonium Lead Iodide

higher temperature is observed for this compound as the symmetry is lost in low temperature regime. The sequence of the phases with respect to the symmetry as a function of decreasing temperature follows the order as cubic \rightarrow tetragonal \rightarrow orthorhombic \rightarrow monoclinic or rhombohedral or hexagonal.¹¹ The stability of $\text{CH}_3\text{NH}_3\text{PbI}_3$ is still a debatable issue. In order to maintain high symmetry cubic structure, the ionic radii of A, B and X species in perovskite structure should satisfy the condition of the tolerance factor t (where $t = (R_A + R_X) / \{\sqrt{2} (R_B + R_X)\}$); here, R_A , R_B and R_X is atomic radii of MA, Pb and I respectively) close to unity. The cubic structure may exist when 't' lies between 0.89 and 1 at finite temperature. The smaller magnitude of 't' leads to lower symmetry such as tetragonal or orthorhombic and larger 't' i.e. $t > 1$ destabilizes bulk network of cubic phase to hexagonal phase that forms layered structure.^{24,25} Moreover, experimentally observed phase of MAPI is found to be tetragonal, whereas the high-throughput computations within the density functional theory framework and thermodynamics predicted orthorhombic phase as more stable phase of MAPI. One of the significant study reported by Zhang et al. in one of the significant study using thermodynamics suggested that the tetragonal phase is unstable and tends to separate phase due to moisture or presence of oxygen in atmosphere.^{26,27} The stability further increases by replacing the Pb by Sn and Cs, but it causes markable decrease in photovoltaic efficiency of the compound. The reason behind to have orthorhombic structure as most stable phase was attributed to the ignorance of long range van der Waals interactions between the molecules and inorganic Pb-I cage as explained by DFT calculations performed at 0 K.²⁷ Recently, using DFT study, it is shown that the most stable /ground state phase is hexagonal phase.²⁸ However, a clear experimental evidence of phase

CHAPTER 6

Two-dimensional Hybrid Inorganic-Organic Perovskites: Methylammonium Lead Iodide

transition from orthorhombic to hexagonal phase or directly from the cubic phase to hexagonal phase is missing. Although, the hexagonal phase is most stable for MAPI, the orthorhombic or tetragonal phase has maintained its importance due to suitable band gap for the photovoltaic cells compared to the hexagonal counterpart which has about 2.6 eV band gap.²⁸ However, the band gap issue can be resolved with 2D perovskite materials as $t > 1$ distorts the cubic structure and further leads to layered geometry. In addition, materials in lower dimensions can provide an excellent combination of structural and photophysical properties after introducing organic ligands between inorganic layered space²⁹ similar to dimension dependent band gap,³⁰ which increases its exciton binding energy and provides better stability compared to bulk counterpart.³¹ The synthesis of organic material based $\text{CH}_3\text{NH}_3\text{SnI}_3$ system with layered geometry is possible which increase hope to have two-dimensional perovskites with layered geometry.³² Moreover, it is shown that when the number of layers tends to infinity, it would ultimately resemble the cubic phase.³² The 2D perovskites are easy to tune for better photophysical and electronic properties due to their flexible structures, stability, decrease in exciton binding energy with increasing inorganic layer and reduced electronic band gap by enhancing hydrogen or halogen bonding between organic cation and inorganic framework.^{32–37} Therefore, these tunable properties of perovskite materials can give new opportunities for photovoltaic applications.

Motivated from the above facts and to understand the role of dimensionality on the electronic properties, optical properties and solar cell parameters, we have investigated these properties of bulk, 2D and 1D MAPI using first principles based DFT computations.³⁸ We have

CHAPTER 6

Two-dimensional Hybrid Inorganic-Organic Perovskites: Methylammonium Lead Iodide

also studied the effect of strain and layer modulation that is, the effect of change in the number of layers or thickness of 2D MAPI on the electronic and optical properties. Our particular interest is to find out the location of conduction/valence band edge states in bulk, 2D and 1D structures of MAPI. Finally, we have used Shockley and Quessier (SQ) model to calculate the solar cell parameters such as, open circuit voltage (V_{oc}), Fill factor (FF), short circuit current density (J_{sc}) and efficiency (η).

6.2 Computational methods

All computations were performed under the umbrella of Kohn-Sham formulated density functional theory (DFT) implemented in planewave pseudopotential simulation package Quantum Espresso.³⁹ The generalized gradient approximation (GGA) parameterized by Perdew, Burke and Ernzerhof (PBE) has been used to treat the exchange and correlation interactions.^{40,41} A kinetic energy cutoff of 150 Ry is used for electronic wave function for bulk, two-dimensional and one-dimensional MAPI. The dense \mathbf{k} -mesh with grid dimensions, $7 \times 7 \times 7$, $7 \times 7 \times 1$ and $7 \times 1 \times 1$ were sampled in reciprocal space for bulk, two-dimensional and one-dimensional MAPI respectively. The Monkhorst-Pack convergence analysis has been utilized to integrate the Brillouin zone (BZ). To achieve better convergence of total energy and forces, the energy convergence value between the two consecutive iterative steps was chosen as 10^{-4} eV and maximum Hellmann-Feynman forces acting on each atom was forced to be less than 0.001 eV/Å. The successful prediction of electronic band gap with different order of dimensional confinement, number of layers and strain in MAPI inspired us to calculate its optical properties.

CHAPTER 6

Two-dimensional Hybrid Inorganic-Organic Perovskites: Methylammonium Lead Iodide

We have calculated the optical properties of bulk, 2D and 1D MAPI using random phase approximation (RPA) with the long wavelength expression utilized for imaginary part of their di-electric tensor.⁴²⁻⁴⁴ We have calculated the absorption coefficient $\alpha = \frac{4\pi E}{hc} \hat{k}(E)$ with h and c as Planck's constant and speed of light respectively and $\hat{k}(E) = \sqrt{(\epsilon_r(\omega)^2 + \epsilon_i(\omega)^2) - \epsilon_r(\omega)}$. The real $\epsilon_r(\omega)$ and imaginary ($\epsilon_i(\omega)$) parts of the di-electric tensor are determined using the Kramers-Kronig relation.³⁸

6.3 Results and discussion

6.3.1 Structural and electronic properties

Before initiating the calculation of the different properties of MAPI under various conditions such as dimensional confinement, with different number of layers and external strain,

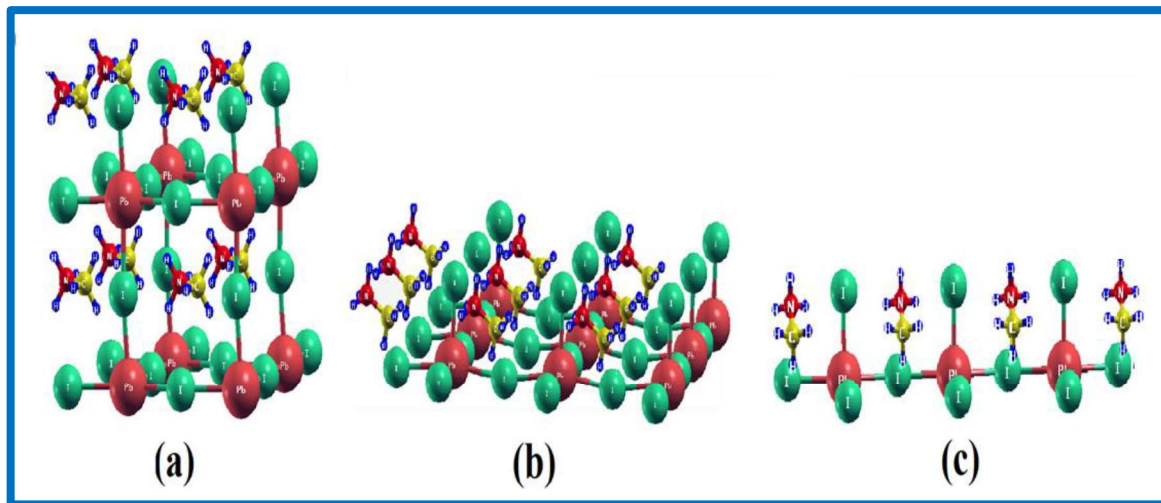


Figure 6.3: Atomic model for the cubic phase of MAPI. (a) bulk, (b) two-dimensional and (c) one-dimensional.

we first optimized the structural parameters of bulk, two-dimensional (2D) and one-dimensional

CHAPTER 6

Two-dimensional Hybrid Inorganic-Organic Perovskites: Methylammonium Lead Iodide

(1D) MAPI separately. The optimized geometries of the same are presented in Fig. 6.3(a-c). For constructing the 2D structures, the vacuum slab of 20 Å height between two MAPI layers in Z direction was introduced; whereas for 1D structure, we introduced vacuum slab of 20 Å thickness along the Y and Z directions for X-directional periodic 1D structure. The computed lattice constants for all considered structures are presented in Table 6.1. We can observe a good

Table -6.1: Calculated lattice constant (Å) and band gap for bulk, two-dimensional and one-dimensional Methylammonium lead iodide (MAPI) in cubic phase along with other available data.

Lattice parameter (Å)	Bandgap (eV)	Electron effective mass(m_e)	Hole effective mass(m_e)
Bulk			
6.46	1.675	0.29	0.31
a=6.28 ⁴⁶ , 6.31 ⁴⁵ , 6.33 ⁴⁸ , 6.39 ⁶⁰ , 6.38 ⁴⁷ , a=b=6.49 c=6.50 ^{47**}	1.53 ⁶⁰ , 1.14 ⁶⁰ , 1.62 ^{48(SR-DFT)} , 1.28 ^{48(SOC-GW)} , 1.69 ^{48(300 K)} , 1.52 ^f	0.35 ⁶¹ 0.18 ^{61(soc)}	0.31 ⁶¹ 0.21 ^{61(soc)}
2D			
a=b=6.383	2.242, 2.24 ⁶²	0.24	0.29
1D			
a=6.38, b=c=20	2.42	0.21	0.27

agreement between the present and available experimental⁴⁵⁻⁴⁸ and theoretical^{24,47,48} data.

The optimization process was followed by the computation of electronic properties by means of electronic band structure calculations. Fig. 6.4(a-c) shows the electronic band structures computed along the high-symmetry directions of the BZ of bulk, 2D and 1D MAPI structures,

CHAPTER 6

Two-dimensional Hybrid Inorganic-Organic Perovskites: Methylammonium Lead Iodide

which clearly indicate an enhancement in the bandgap as a function of the degree of confinement i.e. going from bulk to 2D and to 1D structure. The location of the conduction band minima and

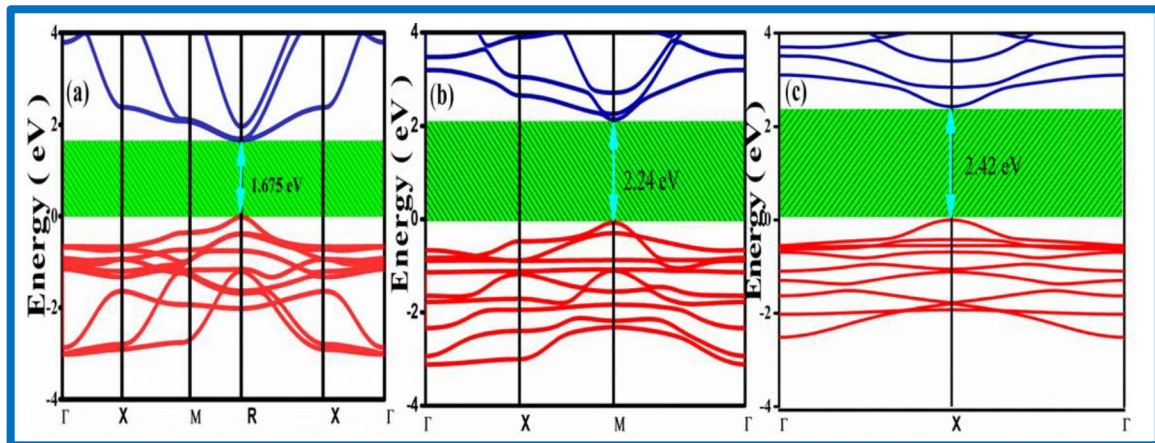


Figure 6.4: Electronic band structure of cubic MAPI. (a) bulk, (b) two-dimensional and (c) one-dimensional MAPI.

valence band maxima depicted in the electronic band structures of the considered systems (see Fig. 6.4(a-c)) reveal that the nature of band gap in MAPI remains unaltered with the order of confinement. The direct bandgap of 1.68 eV at R-point, 2.24 eV at M-point and 2.42 eV at X-point of the BZ is observed for bulk, 2D and 1D MAPI systems respectively. As far as individual atomic orbital contribution is concerned, in the case of bulk MAPI, the valence band mainly consists the contributions from $5s$ and $5p$ orbitals of I and $6d$ and $6s$ orbitals of Pb atoms. The upper most valence band possessing strong anti-bonding states is a result of strong coupling between I p and Pb s orbitals. The contribution of Pb d orbital located within the energy range -3 eV to 0 eV is found to be negligible compared to the remaining atomic orbital contributions. The MA (CH_3NH_3^+) cation does not show any contribution within the energy range of -7 eV to

CHAPTER 6

Two-dimensional Hybrid Inorganic-Organic Perovskites: Methylammonium Lead Iodide

-9 eV which are the dominating band edge states. The conduction band minimum possesses the dominating contributions from Pb *p* and I *s* orbitals. After introducing the one-dimensional confinement in bulk MAPI, i.e. the 2D MAPI system shows a strong anti-bonding coupling between *s* orbital of Pb atom and *p* orbital of adjacent I atom. The contribution of Pb *p* orbital is significantly enhanced in the case of 2D MAPI as compared to its bulk counterpart.

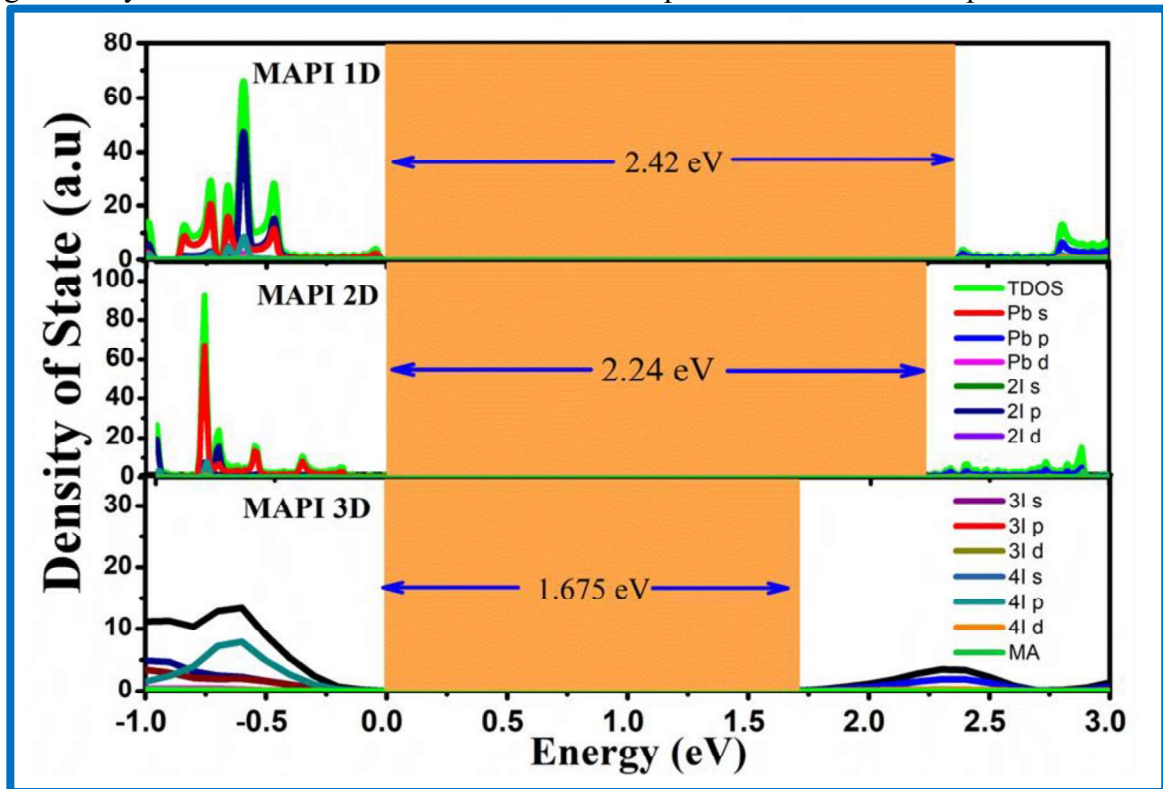


Figure 6.5: Partial electronic density of states (PDOS) for bulk, two-dimensional and one-dimensional MAPI.

To understand the effect of confinement order on electronic band gap of bulk, 2D and 1D MAPI systems, the partial electronic density of states (PDOS) are computed and depicted in Fig. 6.5. We found that the MA ion does not play any direct role in alteration of electronic properties. Furthermore, the orientation of the MA ion in inorganic framework does not affect

CHAPTER 6

Two-dimensional Hybrid Inorganic-Organic Perovskites: Methylammonium Lead Iodide

the transport mechanism of the system; this can be attributed to the weak van der Waals interacting forces acting within the system. The computed ratio of valence band edge state to the conduction band edge state from the DOS plot is found to be highest in case of 1D MAPI, which indicates greater relaxation rates for holes than electrons. Furthermore, the high accumulation of DOS closer to valence band regime is responsible for the generation and transfer of more electrons that in turn causes enhancement in the optical properties of MAPI.

The overall performance of the solar cell depends on the electronic band gap and optical absorption capacity of the device material together with effective mass dependent electronic transport efficiency of carriers. Keeping these factors in view, we computed the effective mass of the electron and hole by applying parabolic fitting to the band edge states along **R-X**, **M- Γ** and **X- Γ** high-symmetry directions for bulk, 2D and 1D MAPI respectively. The magnitude of the effective mass of electron and hole is evaluated using the equation, $m^* = \hbar^2 \left[\frac{\partial^2 \epsilon(k)}{\partial K^2} \right]^{-1}$. The effective mass of the electron and hole in 2D and 1D MAPI is found lower compared to their bulk counterpart due to the presence of flat bands near the band edges. Moreover, balanced effective mass for all cases shows ambipolar condition. The advantage of getting lower effective mass of electron and hole that arises due to the strong *s-p* anti-bonding coupling, is its applicability as a p-i-n configuration. The comparison of all considered MAPI systems suggests that the 2D MAPI is a better candidate for p-i-n configuration for thin-film based solar cells. However, this is not true for 1D MAPI, where the confinement is introduced in two directions. The upper most bands of valence band regime are populated by I *s* orbital with negligible

CHAPTER 6

Two-dimensional Hybrid Inorganic-Organic Perovskites: Methylammonium Lead Iodide

contribution from Pb *d* and Pb *s* orbitals. The *s-p* anti-bonding coupling in 1D MAPI is less as compared to both bulk and 2D MAPI leading to a large enhancement in the magnitude of the band gap. This observation suggests a distinct application of 1D MAPI, particularly in the light emitting diode (LED), field-effect transistor etc.⁴⁹

6.3.2 Implications to solar cell

For a material to be used for solar cell applications, the parameters indicating the real time performance of the solar cell such as open circuit voltage, short circuit current density, fill factor and efficiency^{24,44,50} need to be evaluated. Further, the optimization of the two major factors namely the optical and di-electric properties in case of perovskite based solar cell is reported to be a crucial issue.^{24,50,51} Fig. 6.6(a & b) presents the calculated real $\epsilon_r(\omega)$ and imaginary $\epsilon_i(\omega)$ contributions of the complex di-electric functions for bulk, 2D and 1D MAPI.

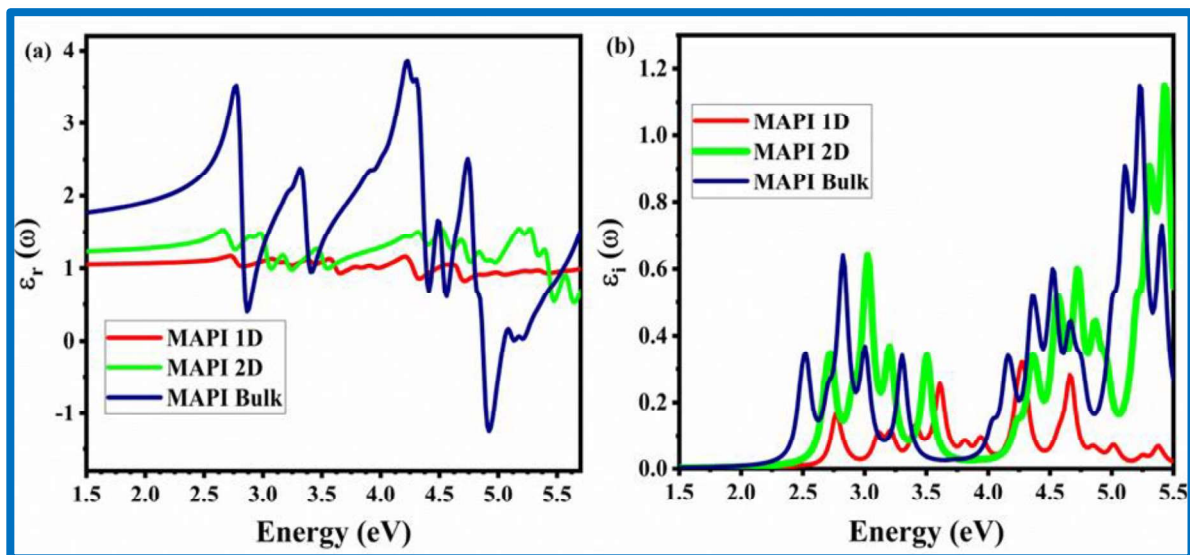


Figure 6.6: (a) Calculated real part of di-electric constant and (b) calculated imaginary part of di-electric constant of bulk, 2D and 1D MAPI.

CHAPTER 6

Two-dimensional Hybrid Inorganic-Organic Perovskites: Methylammonium Lead Iodide

One of the parameters, the absorption coefficient of the material which plays a vital role in the opto-chemical conversion of the solar radiation needs to be within the allowed range of magnitude for solar cell fabrication. The quanta of optical electromagnetic energy with smaller magnitude than the electronic band gap of the host material cannot be absorbed and hence ultimately leads to the loss of precious green energy. The computed di-electric function shows peak in the energy range of 4.2-4.5 eV for all three cases and attains its minima in the range of 4.6-5.0 eV suggesting MAPI to be acting as a transparent surface for high-energy incident photons with metallic nature within the assessed region. The absorption co-efficient which is directly related to the joint density of states (JDOS) of the material under consideration can be computed using di-electric constants. Fig. 6.7(a) presents the absorption profiles of bulk, 2D and

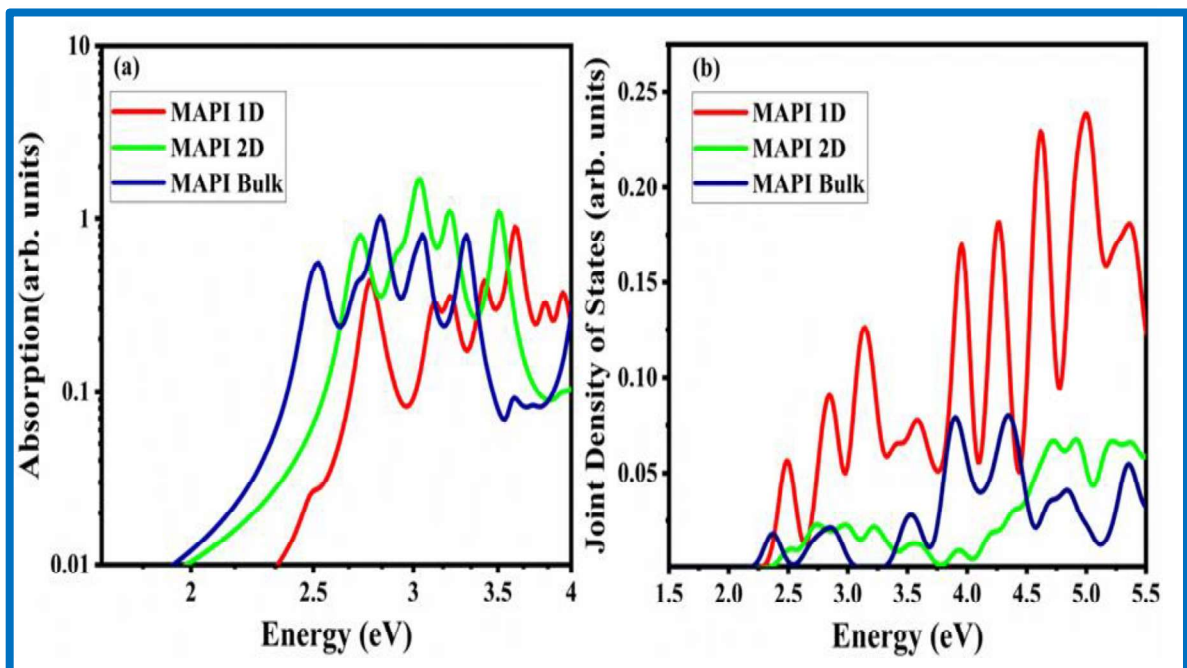


Figure 6.7: (a) Absorption coefficient and (b) joint density of state (JDOS) of bulk, 2D and 1D MAPI.

CHAPTER 6

Two-dimensional Hybrid Inorganic-Organic Perovskites: Methylammonium Lead Iodide

1D MAPI systems. The diagram clearly indicates a blue shift in the response confirming the enhancement in the band gap of 1D MAPI as compared to its bulk and 2D structures. It can be emphasized that in the case of 1D MAPI, higher photon energy is required for photon absorption as compared to the bulk and 2D MAPI. The JDOS plot for 1D MAPI presented in the Fig.6.7(b) shows less absorption efficiency as compared to remaining systems with the highest magnitude observed for the 2D MAPI making it more suitable for solar cell application.

Table-6.2: Calculated Solar cell parameters of bulk, 2D and 1D MAPI with respect to mesoporous (mp)- TiO₂ and PCBM respectively.

System	TiO ₂				PCBM			
	V _{oc} (eV)	FF	J _{sc} (mA/cm ²)	η (%)	V _{oc} (eV)	FF	J _{sc} (mA/cm ²)	η (%)
Bulk	1.14	0.89	21.2	21.5	1.04	0.88	21.2	19.4
	1.04 ⁵⁰	0.73 ⁵⁰	21.3 ⁵⁰	16.2 ⁵⁰	1.07 ⁵⁸	0.59 ⁵⁸	12.5 ⁵⁸	7.89 ⁵⁸
	1.19 ²⁴	0.89 ^{24*}	19.2 ^{24*}	20.33 ^{24*}	1.35 ⁵⁹ (500 nm)	0.91 ⁵⁹ (500 nm)	25.27 ⁵⁹ (500 nm)	30.0 ⁵⁹ (50 0 nm)
	1.35 ⁵⁹ (200 nm)	0.91 ⁵⁹ (200 nm)	22.3 ⁵⁹ (200 nm)	26.8 ⁵⁹ (20 0 nm)	1.305 ⁵ 9(1000 nm)	0.91 ⁵⁹ (100 0 nm)	25.97 ⁵⁹ (1000 nm)	30.88 ⁵⁹ (1 000 nm)
2D	2.15	0.93	11.8	23.6	1.74	0.91	11.8	18.7
1D	1.75	0.92	8.6	13.8	1.17	0.90	8.6	9.1

The results quoted above with the causes and effects discussed in detail clearly show promising electronic and optical properties for 2D MAPI. To ensure that the 2D MAPI is most

CHAPTER 6

Two-dimensional Hybrid Inorganic-Organic Perovskites: Methylammonium Lead Iodide

suitable configuration for solar cell application, we further calculated the solar cell performance parameters such as V_{oc} , FF, J_{sc} and η and presented them in Table 6.2. The V_{oc} is calculated using expression $V_{oc} = E_{LUMO}^{MAPI} - E_{CB}^{TiO_2}$ (for mesoporous (mp)-TiO₂ electrode) and $V_{oc} = |E_{HOMO}^{MAPI}| - |E_{LUMO}^{PCBM}| - 0.3$ (for phenyl C₆₁ or C₇₀ butyric acid methyl ester (PCBM) electrode) [43], where $E_{CB}^{TiO_2}$ and E_{LUMO}^{PCBM} are conduction band minima of TiO₂ and LUMO level of PCBM. The TiO₂ and PCMB are used as mesoporous (mp)-TiO₂ electrode and phenyl C₆₁ or C₇₀ butyric acid methyl ester (PCBM) electrode.^{50,52,53}

In our calculation, we have considered the parameters $E_{CB}^{TiO_2} = 4.0 \text{ eV}$ and $E_{CB}^{TiO_2} = 3.2 \text{ eV}$ [43,44].⁵² Table 6.2 depicts maximum V_{oc} of the order of 1.75 eV, 2.15 eV and 1.14 eV for 1D, 2D and bulk MAPI respectively in case of TiO₂ as a surface substrate material. The calculated V_{oc} is then used to calculate the fill factor using expression $FF = \frac{\vartheta_{oc} - \ln(\vartheta_{oc} + 0.72)}{\vartheta_{oc} + 1}$; $\vartheta_{oc} = \frac{q \times V_{oc}}{K_B T}$.^{54,55} The theoretical J_{sc} (short circuit current density) can be evaluated using the equation $J_{sc} = \int_0^\infty e A(E) I_{sun}(E) dE$; where, I_{sun} is the photon flux density from AM1.5G spectrum and $A(E)$ is absorbance. The attainable current density for a particular bandgap can be obtained by integrating the spectral distribution.

The photovoltaic cell efficiency calculated by Shockley and Quessier (SQ) method is universally accepted due to its dependence on the band gap (E_g) of the material with $A(E) = 1$ for $E \geq E_g$ and $A(E) = 0$ for $E < E_g$. However, under spectroscopic limited maximum efficiency (SLME), the absorbance is thickness dependent and can be evaluated from the

CHAPTER 6

Two-dimensional Hybrid Inorganic-Organic Perovskites: Methylammonium Lead Iodide

equation, $A(E) = 1 - e^{-2\alpha L}$; where α is absorption co-efficient and L is the thickness of the absorbing material.⁵⁶ We use the SQ approximation in our calculation for J_{sc} . The calculated efficiency of solar cell of bulk, 2D and 1D MAPI presented in Table 6.2 is obtained using the formula $\eta = \frac{FF \cdot J_{sc} \cdot V_{oc}}{P_{in}}$; where, P_{in} is the AM1.5 solar irradiation of 100 mW cm^{-2} . Our results on solar cell parameters agree well with earlier reported experimental^{50,57,58} and theoretical^{24,59} values within the constraint of thickness of absorber layer. Our calculated efficiency of 14 % is lower than the efficiency obtained by Sha et al.⁵⁹ This difference is attributed to the use of light

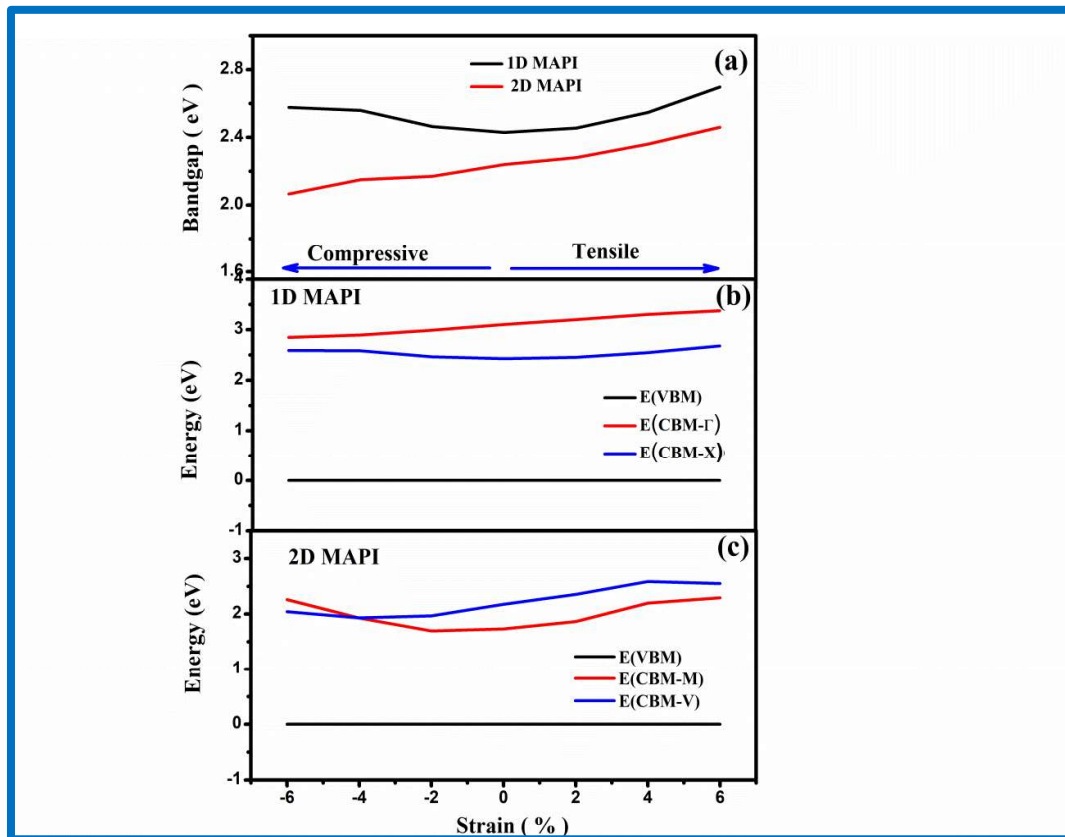


Figure 6.8: (a) Change in bandgap as function of strain, (b) Calculated energies for VBM, CBM at X and CBM at Γ for MAPI 1D as function of uniaxial strain and (c) Calculated energies for VBM, CBM at M and CBM at valley for MAPI 2D as function of biaxial strain.

CHAPTER 6

Two-dimensional Hybrid Inorganic-Organic Perovskites: Methylammonium Lead Iodide

trapping and angular restriction structure using reflecting surface and lower absorber thickness. The efficiency is highest for 2D MAPI followed by bulk and 1D MAPI in case of TiO_2 as surface substrate. These results suggest that the 2D MAPI is one of the most promising candidates for solar cell fabrication.

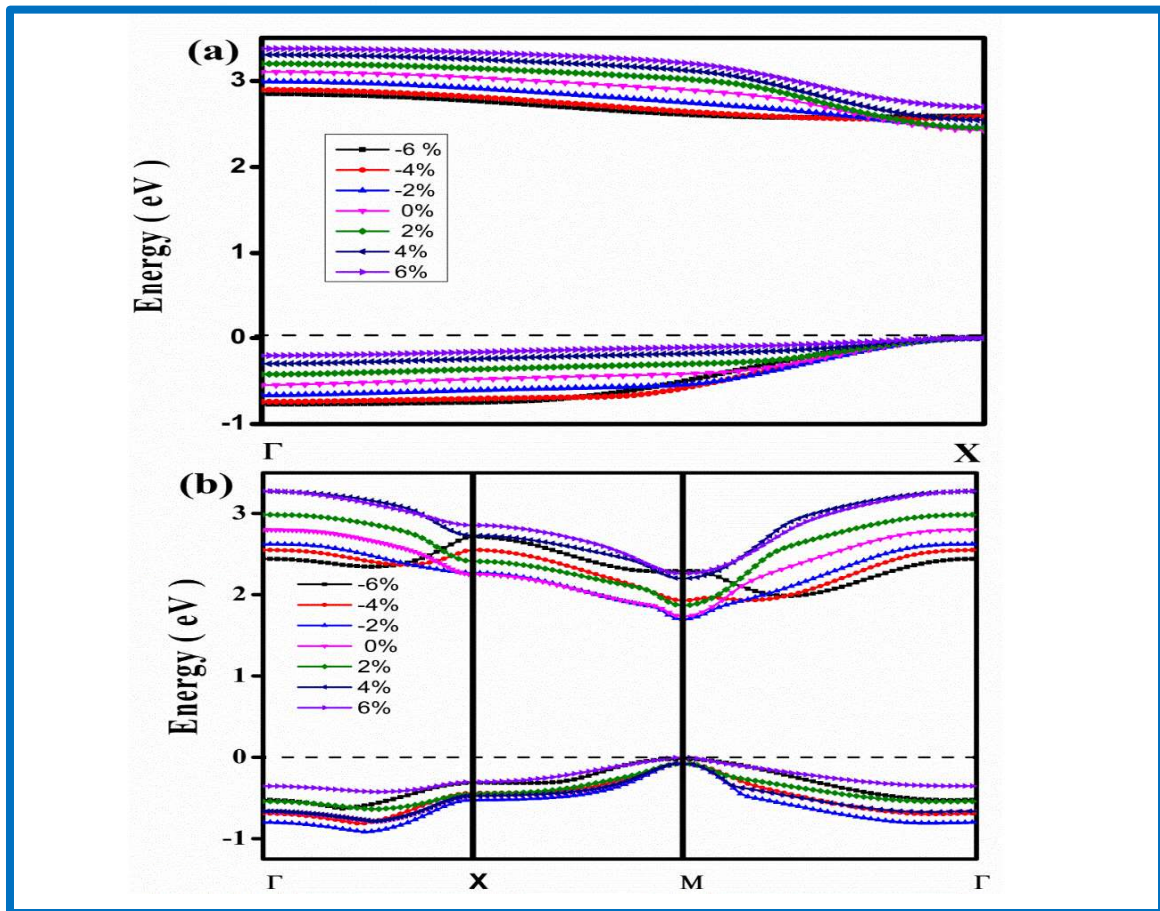


Figure 6.9: (a) Conduction and valence bands of MAPI 1D under different uniaxial strain and (b) Conduction and the valence bands of MAPI 2D under biaxial strain.

The solar performance parameters can be further modulated by tuning the electronic band gap of material. With this motivation, we tuned the electronic properties of MAPI by applying biaxial and uniaxial strains separately on the 2D and 1D MAPI respectively. We have imposed

CHAPTER 6

Two-dimensional Hybrid Inorganic-Organic Perovskites: Methylammonium Lead Iodide

strain magnitudes within the range of -6 % to 6 % for both types of strain. The bandgap variation as a function of external strain is depicted in Fig. 6.8(a). It is clear from the figure that the band gap of 2D MAPI increases on imposing tensile strain (positive strain) and reduces with compressive strain (negative strain). However, in case of 1D MAPI, the band gap increases in both tensile and compressive strains and shows parabolic behavior with strain. It is an interesting observation in both cases; in case of 1D MAPI, direct band gap nature is observed (Fig. 6.9(a)). Moreover, after applying uniaxial strain, an increase in bandgap is found without altering the band nature. We observe indirect to direct bandgap transition in case of 1D MAPI on imposing strain (see Fig. 6.9(a)). Moreover, after applying uniaxial strain, an increase in bandgap is observed without altering the nature of the electronic band gap. It can be clearly observed from Fig. 6.10(b) that the energy of conduction band minima (CBM) at \mathbf{X} (CBM- \mathbf{X}) and CBM at $\mathbf{\Gamma}$ (CBM- $\mathbf{\Gamma}$) increases with respect to strain. The parabolic nature of bandgap versus strain emerges from the parabolic nature of CBM- \mathbf{X} . In case of 2D MAPI, a progressive opening of bandgap upon increasing tensile strain is observed (see Fig. 6.9 and Fig. 6.8(c)) and the nature of the band gap is modified after applying compressive strain as the energy of conduction band minima at \mathbf{M} (CBM- \mathbf{M}) and valley (CBM- \mathbf{V}) crosses each other at -4 % strain i.e. turns to indirect gap in nature. Further, we analyzed the effect of number of layers on the electronic band structure of 2D MAPI and found that on increasing the number of layers, the direct bandgap observed at \mathbf{M} point gradually decreases which is quite obvious as the system approaches to its bulk phase with increasing number of layers. This can be attributed to the presence of the weak van der Waals forces between layers, which increase with the increase in number of layers

CHAPTER 6

Two-dimensional Hybrid Inorganic-Organic Perovskites: Methylammonium Lead Iodide

whereas this interaction is weak in case of monolayer and bilayer. Moreover, the presence of direct band gap nature remains unaffected (see Fig. 6.10) despite increasing the number of layers. This suggests an advantage of multilayer 2D MAPI for optoelectronic application as it will be easier to fabricate stable devices using few layers rather than a monolayer. However, it

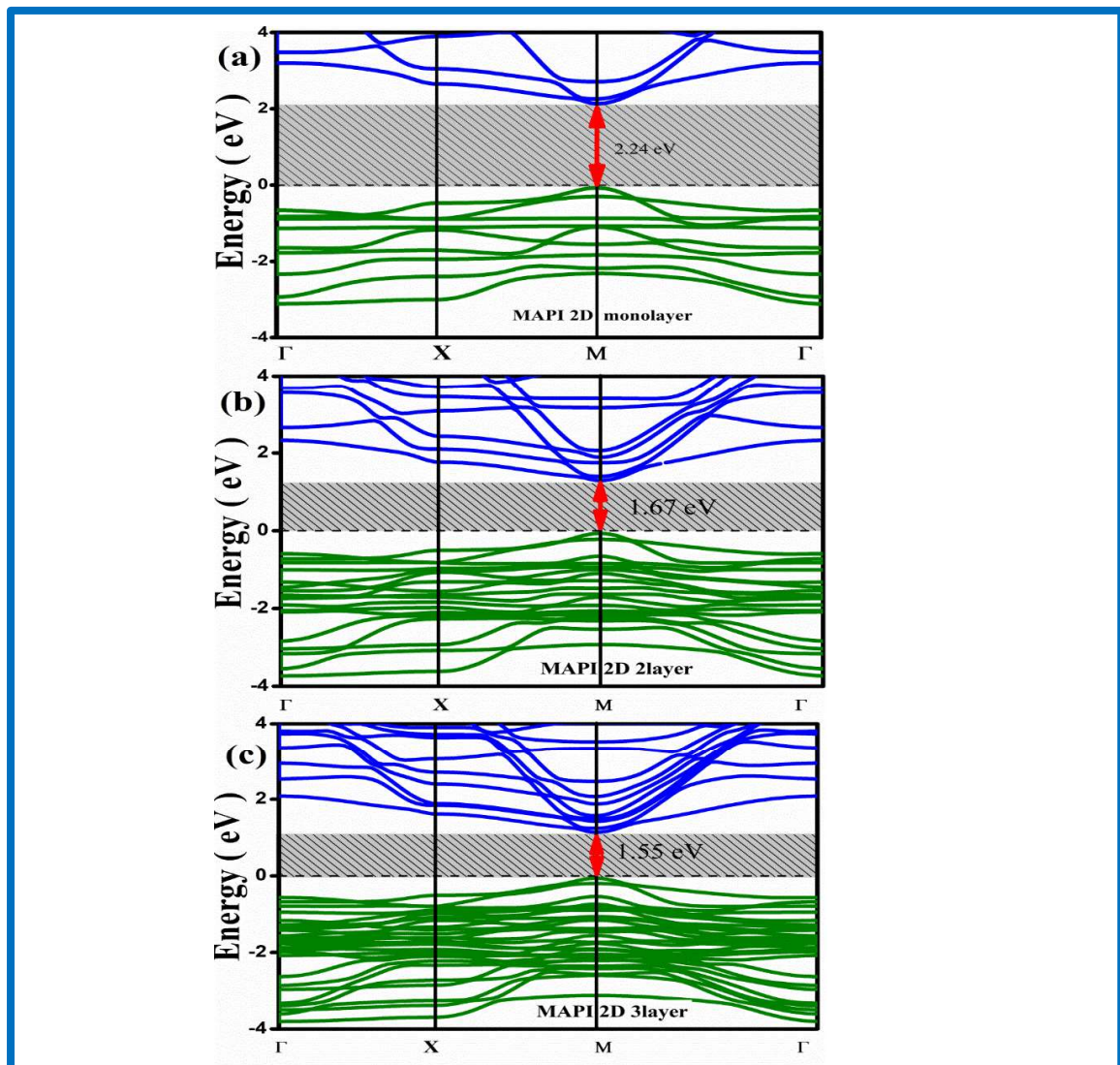


Figure 6.10: Layered electronic band structures of (a) monolayer, (b) bilayer and (c) trilayer of 2D MAPI.

CHAPTER 6

Two-dimensional Hybrid Inorganic-Organic Perovskites: Methylammonium Lead Iodide

is disappointing that the solar cell parameters do not improve with number of layers or with the application of external strain. The magnitude of the band gap increases with while efficiency decreases with external strain while efficiency decreases with external strain overall efficiency (see Table 6.3)

Table 6.3: Solar parameter; open circuit voltage (V_{oc}), fill factor (FF), short circuit current density (J_{sc}) and efficiency (η) of 2D MAPI under strain calculation with respect to mesoporous (mp)- TiO_2 and PCBM respectively.

Strain (%)	TiO_2				PCBM			
	V_{oc} (eV)	FF	J_{sc} (mA/cm ²)	η (%)	V_{oc} (eV)	FF	J_{sc} (mA/cm ²)	η (%)
-6	1.41	0.89	13.04	16.36	1.16	0.89	13.04	13.46
-4	1.38	0.91	11.43	13.87	1.26	0.91	11.43	12.96
-2	1.29	0.90	11.3	13.11	1.37	0.90	11.3	13.93
2	3.00	0.90	9.38	25.32	0.22	0.65	9.38	1.34
4	2.91	0.94	8.1	22.15	0.10	0.49	8.12	0.39
6	2.59	0.93	6.67	16.06	0.27	0.7	6.67	1.27

6.4 Conclusions

In this chapter, we report a systematic study on the electronic properties of methylammonium lead iodide (MAPI) at its different confinement levels i.e. bulk, two-dimensional (2D) and one-dimensional (1D) and their implications to solar cell application by

CHAPTER 6

Two-dimensional Hybrid Inorganic-Organic Perovskites: Methylammonium Lead Iodide

determining the solar cell parameters. The quantum confinement affects the band structure of MAPI and band gap increases as we go from the bulk to 1D MAPI. The CH_3NH_3 (MA) ion plays a major role in tuning the band gap of 2D and 1D MAPI whereas it contributes less in the band structure of bulk MAPI. The density of states of 1D and 2D depict that the holes relaxation rate of 2D and 1D MAPI is much greater compared to their bulk counterpart. The direct to indirect band transition beyond 4% of biaxial compressive strain is observed in the case of 2D MAPI. However, no such effect is observed in the case of 1D MAPI while applying tensile and compressive uniaxial strains. There is a decrease in the band gap of 2D layered MAPI with increase in the number of layers. To understand the photovoltaic properties of 2D MAPI, we have calculated the solar cell parameters such as open circuit voltage, fill factor, short circuit current density and efficiency of solar cell material MAPI in its bulk, 2D and 1D forms. Our study on MAPI reports that the confinement, strain and number of layers (2D case) highly modulate its solar cell parameters. The V_{oc} , FF, J_{sc} and η are highest in case of 2D MAPI followed by the 1D and bulk MAPI. The maximum efficiency of 23.6 % is observed in case of 2D MAPI. The obtained solar cell parameters in the present study is consistent with earlier reports. The present study brings out the fact that the 2D MAPI is best-suited material for solar cell and 2D and 1D MAPI could be useful for future tunable hybrid perovskite-based light emitting diode, photodetectors and solar cells.

CHAPTER 6

Two-dimensional Hybrid Inorganic-Organic Perovskites: Methylammonium Lead Iodide

References

- ¹ Y. Maeno, H. Hashimoto, K. Yoshida, S. Nishizaki, T. Fujita, J.G. Bednorz, and F. Lichtenberg, *Nature* **372**, 532 (1994).
- ² J.B. Torrance, P. Lacorre, A.I. Nazzari, E.J. Ansaldo, and C. Niedermayer, *Phys. Rev. B* **45**, 8209 (1992).
- ³ O. Bohnke, C. Bohnke, J.L. Fourquet, *SolidState Ionics* **91**, 21 (1996)
- ⁴ G.A. Samara, *Ferroelectrics* **2**, 227 (1971).
- ⁵ M.T. Sebastian, *Dielectric Materials for Wireless Communication*, Elsevier (2008).
- ⁶ Z. Cheng and J. Lin, *CrystEngComm* **10**, 2646 (2010).
- ⁷ J.B. Goodenough and M. Longo, "Numerical Data and Functional Relationships in Science and Technology, Group III, Crystal and SSP part a." (1970): 266-274
- ⁸ M.T. Anderson, K.B. Greenwood, G.A. Taylor, and K.R. Poeppelmeier, *Prog. Solid State Chem.* **22**, 197 (1993).
- ⁹ S. Sasaki, C.T. Prewitt, J.D. Bass, and W.A. Schulze, *Acta Crystallogr. Sect. C Cryst. Struct. Commun.* **43**, 1668 (1987).
- ¹⁰ H. Megaw, *A Work. Approach, Stud. Phys. Chem.* **10**, (1973).
- ¹¹ A.M. Glazer, *Acta Crystallogr. Sect. B Struct. Crystallogr. Cryst. Chem.* **28**, 3384 (1972).
- ¹² A.M. Glazer, *Acta Crystallogr. Sect. A* **31**, 756 (1975).
- ¹³ H.D. Megaw, *Proc. Phys. Soc.* **58**, 133 (1946).
- ¹⁴ V.M. Goldschmidt, *Akad. Oslo I. Mat-Nat. K* **18**, 112 (1926).
- ¹⁵ M. Johnsson and P. Lemmens, *Handb. Magn. Adv. Magn. Mater.* **20**, 264001 (2007).
- ¹⁶ T.M. Brenner, D.A. Egger, L. Kronik, G. Hodes, and D. Cahen, *Nat. Rev. Mater.* **1**, 15007 (2016).
- ¹⁷ A.K. Jena, A. Kulkarni, and T. Miyasaka, *Chem. Rev.* **119**, 3036 (2019).
- ¹⁸ L.D. Whalley, J.M. Frost, Y.-K. Jung, and A. Walsh, *J. Chem. Phys.* **146**, 220901 (2017).
- ¹⁹ A. Kojima, K. Teshima, Y. Shirai, and T. Miyasaka, *J. Am. Chem. Soc.* **131**, 6050 (2009).

CHAPTER 6

Two-dimensional Hybrid Inorganic-Organic Perovskites: Methylammonium Lead Iodide

- ²⁰ H. Zhou, Q. Chen, G. Li, S. Luo, T. -b. Song, H.-S. Duan, Z. Hong, J. You, Y. Liu, and Y. Yang, *Science* **345**, 542 (2014).
- ²¹ A. Poglitsch and D. Weber, *J. Chem. Phys.* **87**, 6373 (1987).
- ²² P.S. Whitfield, N. Herron, W.E. Guise, K. Page, Y.Q. Cheng, I. Milas, and M.K. Crawford, *Sci. Rep.* **6**, 1 (2016).
- ²³ C.-J. Yu, *J. Phys. Energy* **1**, 22001 (2019).
- ²⁴ W.-J. Yin, J.-H. Yang, J. Kang, Y. Yan, and S.-H. Wei, *J. Mater. Chem. A Mater. Energy Sustain.* **3**, 8926 (2015).
- ²⁵ R. Søndenå, S. Stølen, P. Ravindran, T. Grande, and N.L. Allan, *Phys. Rev. B - Condens. Matter Mater. Phys.* **75**, 184105(2007).
- ²⁶ Y.-Y. Zhang, S. Chen, P. Xu, H. Xiang, X.-G. Gong, A. Walsh, and S. Wei, *Nat. Commun.* **11**, (2015).
- ²⁷ Y.-Y. Zhang, S. Chen, P. Xu, H. Xiang, X.-G. Gong, A. Walsh, and S.-H. Wei, *Chinese Phys. Lett.* **35**, 36104 (2018).
- ²⁸ A.S. Thind, X. Huang, J. Sun, and R. Mishra, *Chem. Mater.* **29**, 6003 (2017).
- ²⁹ D.B. Mitzi, C.A. Feild, W.T.A. Harrison, and A.M. Guloy, *Nature* **369**, 467 (1994).
- ³⁰ T. Ishihara, J. Takahashi, and T. Goto, *Solid State Commun.* **69**, 933 (1989).
- ³¹ J. Yang, B.D. Siempelkamp, D. Liu, and T.L. Kelly, *ACS Nano Advance* **9**, 1955 (2015).
- ³² D.B. Mitzi, *J. Chem. Soc. Dalt. Trans.* **1**, 1 (2001).
- ³³ T. Ishihara, *J. Lumin.* **60**, 269 (1994).
- ³⁴ S. Sourisseau, N. Louvain, W. Bi, N. Mercier, D. Rondeau, F. Boucher, J.-Y. Buzaré, and C. Legein, *Chem. Mater.* **19**, 600 (2007).
- ³⁵ J.L. Knutson, J.D. Martin, and D.B. Mitzi, *Inorg. Chem.* **44**, 4699 (2005).
- ³⁶ N. Mercier, S. Poiroux, A. Riou, and P. Batail, *Inorg. Chem.* **43**, 8361 (2004).
- ³⁷ D.B. Mitzi, *Chem. Mater.* **8**, 791 (1996).
- ³⁸ N.N. Som, P. Sampath, S.D. Dabhi, V. Mankad, S. Shinde, M.L.C. Attygalle, and P.K. Jha, *Sol. Energy* **173**, 1315 (2018).

CHAPTER 6

Two-dimensional Hybrid Inorganic-Organic Perovskites: Methylammonium Lead Iodide

- ³⁹ P. Giannozzi, S. Baroni, N. Bonini, M. Calandra, R. Car, C. Cavazzoni, D. Ceresoli, G.L. Chiarotti, M. Cococcioni, I. Dabo, A. Dal Corso, S. De Gironcoli, S. Fabris, G. Fratesi, R. Gebauer, U. Gerstmann, C. Gougoussis, A. Kokalj, M. Lazzeri, L. Martin-Samos, N. Marzari, F. Mauri, R. Mazzarello, S. Paolini, A. Pasquarello, L. Paulatto, C. Sbraccia, S. Scandolo, G. Sclauzero, A.P. Seitsonen, A. Smogunov, P. Umari, and R.M. Wentzcovitch, *J. Phys. Condens. Matter* **21**, (2009).
- ⁴⁰ J. Perdew, K. Burke, and M. Ernzerhof, *Phys. Rev. Lett.* **77**, 3865 (1996).
- ⁴¹ J.P. Perdew and K. Burke, *Phys. Rev. B - Condens. Matter Mater. Phys.* **54**, 16533 (1996).
- ⁴² M. Gajdoš, K. Hummer, G. Kresse, J. Furthmüller, and F. Bechstedt, *Phys. Rev. B* **73**, 045112 (2006).
- ⁴³ J. Harl, G. Kresse, L.D. Sun, M. Hohage, and P. Zeppenfeld, *Phys. Rev. B* **76**, 20 (2007).
- ⁴⁴ M. Bercx, N. Sarmadian, R. Saniz, B. Partoens, and D. Lamoen **18**, 20542 (2016).
- ⁴⁵ T. Baikie, Y. Fang, J.M. Kadro, M. Schreyer, F. Wei, S.G. Mhaisalkar, M. Graetzel, and T.J. White, *J. Mater. Chem. A* **1**, 5628 (2013).
- ⁴⁶ C.C. Stoumpos, C.D. Malliakas, and M.G. Kanatzidis, *Inorg. Chem.* **52**, 9019 (2013).
- ⁴⁷ D.A. Egger and L. Kronik, *J. Phys. Chem. Lett.* **5**, 2728 (2014).
- ⁴⁸ C. Quarti, E. Mosconi, J.M. Ball, V. D’Innocenzo, C. Tao, C. Pathak, A. Petrozza, H. Snaith, F. De Angelis, S. Pathak, A. Petrozza, H. Snaith, and F. De Angelis, *Energy Environ. Sci.* **16**, 155 (2015).
- ⁴⁹ M. Spina, M. Lehmann, B. Náfrádi, L. Bernard, E. Bonvin, R. Gaál, A. Magrez, L. Forró, and E. Horváth, *Small* **11**, 4824 (2015).
- ⁵⁰ S. Ryu, J.H. Noh, N.J. Jeon, Y.C. Kim, W.S. Yang, J. Seo, and S. Il Seok, *Energy Environ. Sci.* **7**, 2614 (2014).
- ⁵¹ Q. Zhou, D. Jiao, K. Fu, X. Wu, Y. Chen, J. Lu, and S. Yang, *Sol. Energy* **123**, 51 (2016).
- ⁵² M. Bourass, A. Fitri, A. Touimi Benjelloun, M. Benzakour, M. Mcharfi, M. Hamidi, F. Serein-Spirau, T. Jarrosson, J.P. Lère-Porte, J.M. Sotiropoulos, and M. Bouachrine, *Der Pharma Chem.* **5**, 144 (2013).
- ⁵³ A. El alamy, M. Bourass, A. Amine, M. Hamidi, and M. Bouachrine, *Karbala Int. J. Mod. Sci.* **3**, 75 (2017).
- ⁵⁴ M.A. Green, A. Ho-Baillie, and H.J. Snaith, *Nat. Photonics* **8**, 506 (2014).

CHAPTER 6

Two-dimensional Hybrid Inorganic-Organic Perovskites: Methylammonium Lead Iodide

- ⁵⁵ M. Leilaeioun and Z.C. Holman, *J. Appl. Phys.* **120**, 123111 (2016).
- ⁵⁶ L. Yu and A. Zunger, *Phys. Rev. Lett.* **108**, 1 (2012).
- ⁵⁷ Q. Chen, H. Zhou, Z. Hong, S. Luo, H.S. Duan, H.H. Wang, Y. Liu, G. Li, and Y. Yang, *J. Am. Chem. Soc.* **136**, 622 (2013).
- ⁵⁸ I. Gelmetti, L. Cabau, N.F. Montcada, and E. Palomares, *ACS Appl. Mater. Interfaces* **9**, 21599 (2017).
- ⁵⁹ W.E.I. Sha, X. Ren, L. Chen, W.C.H. Choy, W.E.I. Sha, X. Ren, L. Chen, and W.C.H. Choy, *Appl. Phys. Lett.* **106**, 221104, (2015).
- ⁶⁰ J.M. Frost and A. Walsh, *Acc. Chem. Res.* **49**, 528 (2016).
- ⁶¹ W.J. Yin, T. Shi, and Y. Yan, *Adv. Mater.* **26**, 4653 (2014).
- ⁶² D.H. Cao, C.C. Stoumpos, O.K. Farha, J.T. Hupp, and M.G. Kanatzidis, *J. Am. Chem. Soc.* **137**, 7843 (2015).